Role of the Solvent in Computing the 1,4-Benzosemiquinone g-Tensor by the Coupled-Perturbed Kohn−Sham Hybrid Density Functional Method†

Saba M. Mattar*

Department of Chemistry, University of New Brunswick, Fredericton, New Brunswick, Canada E3B6E2

Received: November 6, 2003; In Final Form: March 15, 2004

The 1,4-benzosemiquinone (BzSQ) **g**-tensor components, in the gas phase and in methanol, are computed. Neese's coupled-perturbed Kohn−Sham method is used, in conjunction with the UB1LYP and UPBE0 exchange-correlation hybrid density functionals. The computed **g**-tensor elements are analyzed and broken down into their individual first- and second-order contributions. The inclusion of electron correlation, via the UB1LYP and UPBE0 hybrid density functionals, improves these calculations over those carried out at the Hartree−Fock level. Further improvement is obtained if the SCF reaction field method (SCRF) of Tomasi, as implemented by Barone, is employed to mimic the solvent effects. The best agreement with experiment is achieved using a model in which the BzSQ hydrogen bonds to four methanol solvent molecules to form a supermolecule. This occurs because the main contribution to the **g**-tensor components arises from the net spin densities on the carbonyl oxygen atoms, which are highly influenced by hydrogen bonding with the solvent. Thus, provided the solvent effects are explicitly included, the calculated **g**-tensor components are in very good agreement with the corresponding experimental values. BzSQ in the gas phase has D_{2h} symmetry and a $^2B_{2g}$ ground state with no off-diagonal **g**-tensor components. Hydrogen bonding to the four methanol molecules reduces its symmetry to D_2. However, a group theoretical analysis reveals that there should be no shift in the directions of the **g**-tensor principal axes due to hydrogen bonding. Finally, the isotropic ^{1}H hyperfine coupling constants, obtained by these calculations, are also in excellent agreement with their experimental counterparts.

1. Introduction

Electron paramagnetic resonance (EPR) is a powerful spectroscopic tool for the study of the structure, function, and dynamics of biological systems containing free radicals. It has been known for some time that biological electron-transfer reactions, such as respiration and photosynthesis, involve semiquinones and their corresponding radical anions.[1] For example, in the initial stages of photosynthesis a charge separation occurs by forming a chlorophyll radical cation and a 1,4-semiquinone radical anion.[2] For the past 40 years EPR spectroscopy has been used to determine the hyperfine (**A**) and gyromagnetic (**g**) tensors of semiquinone free radicals.[3,4] To understand the magnetic properties of biological semiquinones, such as the ubiquinone and plastoquinone radical anions, it is logical to start with 1,4-benzosemiquinone (BzSQ) since it constitutes the simplest building block of such radicals.

In general, it is ideal to correlate the BzSQ's experimental **A**- and **g**-tensor components with the corresponding values calculated theoretically. When a good correlation between theory and experiment is found, a clear picture of the net spin density distribution, spin−orbit coupling, and electronic structure-bonding relationships of these radical anions emerges. In addition, the experimental **g** and **A** tensors are best determined by simulation of their EPR spectra. Ideally, the computed **A**- and **g**-tensor components should be used as an a priori initial guess in the simulations. Then they are subsequently refined until the experimental and simulated spectra match one another.

The theoretical computations of **A**-tensor components are more prevalent in the literature than those of the **g** tensors. Ab initio Hartree−Fock methods have been disappointing in their ability to predict the magnitude and signs of **A** tensors.[5] Alternatively, hybrid density functional (HDF) methods, when used with moderate basis sets, have been very successful in computing the optimal geometries, vibrational frequencies, and electronic structures of molecules with ground states that are described by a predominant single determinant.[5,6] Recently, the HDF methods, which have the advantage of containing no adjustable parameters, have been introduced.[7] They give more accurate isotropic hyperfine tensor values than the older and more commonly used B3LYP HDF.[7−10] Improta and Barone give an exhaustive review of how electronic, environmental, and vibrational effects influence the computation of the magnetic properties of free radicals using hybrid density functional methods.[11]

In EPR the **g** tensor plays an important role equivalent to the chemical shift tensor, σ, in solid-state nuclear magnetic resonance spectroscopy. Most spin labeled proteins and biological free radical studies involve the monitoring of the **A** and **g** tensors in different environments and solvents. Thus, calculating the **g**-tensor components in these media would be a definite asset.

The main development of the **g** tensor theory was undertaken by Stone.[12] There are also excellent reviews on the subject by McWeeny[13] and Harriman.[14] In particular, Pilbrow's book gives a comprehensive account of the **g** tensor of transition metal complexes.[15] According to Stone, organic radical anions have higher **g** values than their corresponding cations.[12] In this context, **g** values may be used as indicators of the effective

† Part of the special issue "Jack H. Freed Festschrift".

* E-mail: mattar@unb.ca. Telephone: +1 (506) 447 3091. Fax: +1 (506) 453 4981.

10.1021/jp031230d CCC: $27.50
Published on Web 04/22/2004

charge of the free radical.[16] Furthermore, one of the essential steps in determining an electron−nuclear double resonance (ENDOR) spectrum of a free radical is to first set the applied magnetic field to coincide with one of the **g** tensor principal axes, g_{xx}, g_{yy}, and g_{zz}. Knowing the magnitudes and orientation of g_{xx}, g_{yy}, and g_{zz} relative to the radical's inertial axes beforehand is very helpful in ENDOR spectroscopy.

The **g** tensor anisotropy of organic free radicals is small compared to inorganic complexes. This is due to the small spin−orbit coupling constants of H, C, N, and O compared to those of transition metals. Therefore in biological systems, the X-band (≈9.0 GHz) EPR spectra of immobilized and randomly oriented organic free radicals usually are not well resolved and thus yield limited information about these tensors.[17] Their corresponding ENDOR spectra are somewhat more informative and permit the determination of some hyperfine tensor components.[18−20] Alternatively, the resolution of an organic radical's **g**-tensor anisotropy in an EPR spectrum may be increased by using EPR spectrometers that operate at higher frequencies, such as 18.0 GHz (P-band),[21] 35 GHz (Q-band), 95 GHz,[22] and 150 GHz[23] etc. Freed and co-workers, in addition to designing a P-band spectrometer,[21] were the first to use quasi-optical components to construct a 250 GHz spectrometer.[24]

The experimental EPR spectrum of BzSQ was determined, at 9 GHz, by Freed.[4] Hales recorded its spectrum at 35 GHz in methanol;[17] Burghaus et al. recorded the spectrum at 95 GHz in 2-propanol.[22] The **g**-tensor components in the 95 GHz EPR spectrum were almost totally resolved and were experimentally determined with a high degree of accuracy.[22] O'Malley was the first to use the B3LYP hybrid density functional method to calculate the ^{1}H, ^{13}C, and ^{17}O isotropic hyperfine coupling constants of the BzSQ radical anion. He found very good agreement between the experimental and computed hyperfine tensor components.[25]

In the past, **g**-tensor components have been calculated using semiempirical,[12,22,26] ab initio,[27,28] density functional,[29−31] and hybrid density functional methods.[32] In most cases, the conventional ab initio sum-over-states method to compute the second-order contributions to the **g** tensor[27] for molecules larger than triatomics is cumbersome and impractical.[28] A large number of low lying excited states must be explicitly calculated. For practical reasons, the second-order perturbation contributions from excited states should be truncated at some predetermined point. It is not always guaranteed that the included contributions are enough to ensure convergence. These problems are accentuated as the paramagnetic molecule increases in size. To overcome these obstacles Vahtras et al. used an alternative method based on linear multiconfiguration response theory. In their method, contributions from all intermediate states are implicit in the calculations.[28]

To the best of our knowledge, there has been one computation of the BzSQ **g**-tensor components by Engstrom et al. which utilized the linear response method at the restricted Hartree−Fock level in the gas phase.[33] The authors determined that the carbonyl bond length greatly influenced the computed **g** tensors. They then computed the **g**-tensor components as a function of each of the CO, C2C3, and C1C2 bond lengths shown in Figure 1. Even with this geometrical flexibility they concluded that electron−electron correlation may be necessary to improve the agreement between the experimental and computed **g** tensors.[33] This would take into consideration the strong coupling and correlation of the ground and low lying excited states. Although they predicted that hydrogen bonding and polar solvents may also influence the **g** tensor components, they did not include these effects in their computations.[33]

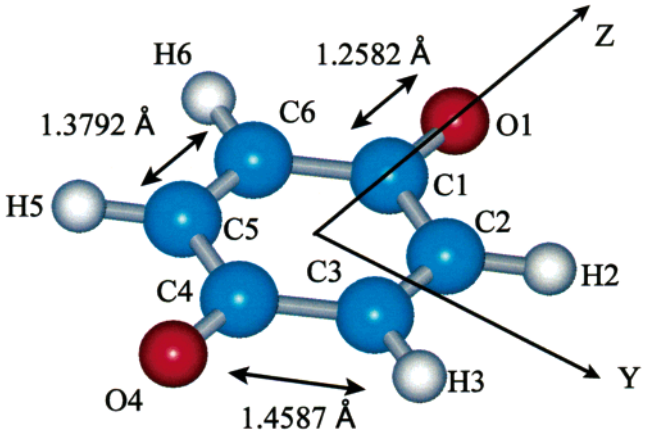

Figure 1. Geometry, atom numbering, orientation, and bond lengths of the 1,4-benzosemiquinone (BzSQ) radical anion.

In this article we attempt to improve the agreement between the experimental and computed **g** tensors of BzSQ. The UPBE0 and UB1LP hybrid density functionals, containing correlation effects, are used rather than the simpler Hartree−Fock method. The sum-over-states technique is avoided by utilizing Neese's coupled-perturbed Kohn−Sham (CPKS) method[32] to independently determine the radical's experimental **g**-tensor components. Furthermore, the effects of the solvent and the environment are included in two different ways. In the first, Tomasi's reaction field formalism, as implemented by Barone, is used to mimic the solvent effects.[34−38] In the second, a supermolecule is constructed by optimizing the geometry of the BzSQ radical anion and four hydrogen bonded methanol solvent molecules.

2. Computational Details

All computations were performed with the GAUSSIAN 03W suite of programs.[39] Since the X-ray crystal structure for BzSQ is not known, its geometry in the gas phase and when interacting with four methanol molecules was optimized using the UB1LYP HDF method and the double-ζ EPR−II basis set. The resulting optimal geometries did not have any imaginary vibrational frequencies that are characteristic of transition states or saddle points on the energy surfaces. They were then used to compute the **g**-tensor components, using the UB1LYP and UPBE0 hybrid density functionals.[7,40,41]

To test the effect of the basis sets on the magnitude of the BzSQ **g**-tensor components, Barone's EPR−II and EPR−III basis sets[42] and Dunning's larger, augmented correlation-consistent triple-ζ polarization basis sets (Aug-cc-pVTZ)[43] were used for most of the computations. To include the effects of the methanol solvent, Tomasi's polarized continuum method (PCM) was employed, whereby the molecules are placed into a solvent cavity with the dielectric constant, $\epsilon = 32.63$, for methanol. The cavity is constructed from a series of interlocking spheres.[34−38]

3. Results and Discussion

3a. Numerical Computation of the g-Tensor Components. The geometry optimization of the BzSQ radical in the gas phase using the UB1LYP HDF and the EPR−II basis set resulted in a CO bond length of 1.2582 Å. This is depicted in Figure 1 along with the C1C2 and C2C3 bond lengths.

Inspection of Table 1 shows that the experimental BzSQ **g**-tensor components, measured at 95 GHz in 2-propanol are

TABLE 1: 1,4-Benzosemiquinone Experimental and Computed Principal g-Tensors

basis	g_{xx}	g_{yy}	g_{zz}	$\langle g \rangle$	g_{zz}	g_{yy}	g_{xx}	$\langle g \rangle$
			experimental					
	2-propanol, W−band[a]				methanol, Q-band[b]			
	2.00229	2.00526	2.00645	2.00467	2.0023	2.0053	2.0065	2.0047
			computed					
gas phase[c]			UHF					
EPR−II	2.00216	2.00727	2.00992	2.00645				
EPR−III	2.00217	2.00767	2.01067	2.00684				
AUG-cc-pVTZ	2.00217	2.00709	2.00947	2.00624				
Gas Phase[c]			UB1LYP				UPBE0	
EPR−II	2.00214	2.00583	2.00918	2.00572	2.00214	2.00582	2.00930	2.00575
EPR−III	2.00215	2.00642	2.01042	2.00633	2.00214	2.00637	2.01047	2.00633
AUG-cc-pVTZ	2.00214	2.00586	2.00906	2.00569	2.00214	2.00583	2.00912	2.00570
UAHF−SCRF−PCM-CH_3OH[c]			UB1LYP				UPBE0	
EPR−II	2.00214	2.00563	2.00838	2.00538	2.00214	2.00564	2.00850	2.00543
EPR−III	2.00215	2.00609	2.00913	2.00579	2.00214	2.00606	2.00922	2.00581
AUG-cc-pVTZ	2.00214	2.00564	2.00812	2.00530	2.00214	2.00562	2.00821	2.00532
BzSQ·$4CH_3OH$[c,d]			UB1LYP				UPBE0	
EPR−II	2.00218	2.00547	2.00717	2.00494	2.00218	2.00545	2.00718	2.00494
AUG-cc-pVTZ	2.00218	2.00548	2.00707	2.00491				

[a] Reference 22. Due to the D_{2h} symmetry of these $^2B_{2g}$ radicals, the total **g** tensor has no off-diagonal components. [b] Reference 17. [c] This work. [d] Supermolecule has D_2 symmetry and a $^2B_2$ ground state.

listed with one more significant figure than those measured at 35 GHz in methanol. Otherwise, the g_{xx}, g_{yy}, and g_{zz} components are essentially the same. The computed **g**-tensor components, using the optimized geometry, at the unrestricted Hartree−Fock (UHF) level and EPR−II basis are given in Table 1. From this table one observes that, in comparison to the experimental values, the calculation overestimates both the g_{yy} and g_{zz} values by 2010 and 3470 ppm, respectively. On the other hand, the g_{xx} component is slightly less than the experimental one. At the UHF/EPR−III level, the g_{xx} component remains essentially the same, but the g_{yy} and g_{zz} values are poorer. They now differ from the experimental ones by 2410 and 4220 ppm. Recalculation of the **g** values with Dunning's larger AUG-cc-pVTZ basis sets resulted in $g_{xx} = 2.00217$, $g_{yy} = 2.00709$, and $g_{zz} = 2.00947$. These are in better agreement with experiment but still larger than the experimental g_{yy} and g_{zz} values. It is important to note that while the g_{yy} and g_{zz} are overestimated by the coupled-perturbed Hartree−Fock method[32] used here, the corresponding values are underestimated by the linear response method.[33]

To include the effects of correlation in the computations, one resorts to the UB1LYP[7] and UPBE0[41] hybrid density functionals. The resulting **g**-tensor components for BzSQ in the gas phase are also listed in Table 1. These results show the same trends observed by their UHF counterparts. Specifically, both the g_{yy} and g_{zz} are still overestimated and the g_{xx} is slightly lower than the experimental value. For example, the UB1LYP/EPR−III calculation resulted in **g**-tensor components that are in poorer agreement with experiment than the UB1LYP/EPR−II values, and the AUG-cc-pVTZ set gave improved results over both the EPR−II and EPR−III basis sets. On the whole, the inclusion of electron correlation effects, via the B1LYP and UPBE0 functionals, caused all **g**-tensor values to be closer to the experimental values than corresponding ones obtained using the simpler UHF technique. Thus one may conclude that hybrid density functionals give slightly better **g**-tensor values than the pure UHF method.

The next logical step is to compensate for solvent effects in a relatively efficient manner. This is accomplished by employing Tomasi's UAHF−SCRF−PCM method to mimic the methanol environment.[34−38] The computed **g**-tensor components, listed in Table 1, still indicate the same trends as those of the UHF, UB1LYP, and UPBE0 in the gas phase. In addition, the UAHF−SCRF−PCM computations are even closer to the experimental ones than the previous gas-phase results.

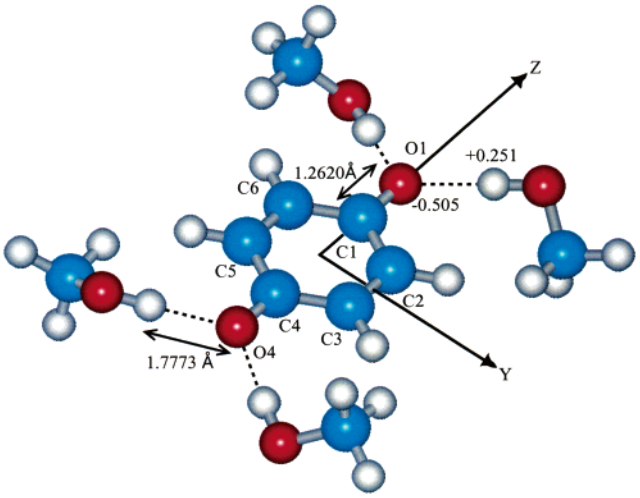

Figure 2. Orientation and geometry of BzSQ hydrogen bonded to four methanol solvent molecules. The overall BzSQ·$4CH_3OH$ system has D_2 symmetry. The figure also depicts the CO bond length and the distance between the O1 atom of the BzSQ and the hydrogen atom of the methanol hydroxyl group. The charges on these atoms are −0.505 and 0.251, respectively.

Logically the **g**-tensor components should be influenced by both the polarity and hydrogen bonding of the solvent. In addition to the bulk solvent properties, such as the dielectric constant, specific solute−solvent interaction should also be considered.[11] In an effort to get even more improvement between the experimental and computed **g**-tensor components, BzSQ and four methanol molecules were geometry optimized as a single supermolecule, BzSQ·$4CH_3OH$. In the resulting system, shown in Figure 2, the BzSQ molecule is hydrogen bonded via each of its carbonyl oxygen atoms to two hydrogen atoms from the OH groups of two methanols. The four methanol moieties are symmetrically positioned around the BzSQ radical and the supermolecule has D_2 symmetry. As a result of this hydrogen bonding, the CO bond lengths increase from 1.5282 to 1.6260 Å. The hydrogen bond length is found to be 1.7773 Å. The negative charge on the carbonyl oxygen is −0.505, while that

TABLE 2: Individual Contribution to the Total g-Tensor Components of BzSQ·4CH$_3$OH

BzSQ·4CH$_3$OH	UB1LYP/EPR−II				UB1LYP/AUG-cc-pVTZ		
$\Delta g^{RMC}\delta_{rs}$	*x*	*y*	*z*		*x*	*y*	*z*
x	-0.23895×10^{-3}	0.00	0.00	*x*	-0.23619×10^{-3}	0.00	0.00
y	0.00	-0.23895×10^{-3}	0.00	*y*	0.0	-0.23619×10^{-3}	0.00
z	0.00	0.00	-0.23895×10^{-3}	*z*	0.0	0.00	-0.23619×10^{-3}
Δg_{rs}^{GC}	*x*	*y*	*z*				
x	0.25158×10^{-4}	0.00	0.00	*x*	0.29869×10^{-4}	0.00	0.00
y	0.00	0.45288×10^{-4}	0.00	*y*	0.0	0.55654×10^{-4}	0.00
z	0.00	0.00	0.15401×10^{-3}	*z*	0.0	0.00	0.14617×10^{-3}
$\Delta g_{rs}^{OZ/SOC}$	*x*	*y*	*z*				
x	0.69685×10^{-4}	0.00	0.00	*x*	0.95267×10^{-4}	0.00	0.00
y	0.00	0.33402×10^{-2}	0.00	*y*	0.0	0.33436×10^{-2}	0.00
z	0.00	0.00	0.49311×10^{-2}	*z*	0.0	0.00	0.48442×10^{-2}
g_{rs}^{total}	*x*	*y*	*z*				
x	2.00218	0.00	0.00	*x*	2.00218	0.00	0.00
y	0.00	2.00547	0.00	*y*	0.0	2.00548	0.00
z	0.00	0.00	2.00717	*z*	0.0	0.00	2.00707

on each of the methanol hydroxy hydrogens is 0.251. Although the incorporation of a limited number of methanol molecules in the computations is not a perfect solution, it should account for a significant part of the solvent effects.[25]

Despite the fact that the BzSQ geometry seems to change slightly in going from the gas phase to being hydrogen bonded to four methanols, the computed **g**-tensor components change significantly. The results of the computations listed in Table 1 reveal that, when compared to the gas-phase values, the g_{xx}, g_{yy}, and g_{zz} components of the BzSQ·4CH$_3$OH supermolecule are closer to the experimental values by 40, 190, and 2010 ppm, respectively. Thus the charge redistribution and increase in CO bond lengths, due to hydrogen bonding with the solvent, play pivotal roles.

It is generally accepted that the accuracy of the **g**-tensor components determined by simulation of the experimental spectrum is within one part per thousand.[32] The computed g_{xx}, g_{yy}, and g_{zz} components of the BzSQ·4CH$_3$OH by the UB1LYP/AUG-cc-pVTZ method differ from the corresponding experimental values by 110, 220, and 620 ppm, respectively. Thus, one can conclude that there is very good agreement with experiment.

3b. Individual Contributions to the g-Tensor Components. Having obtained very good agreement with experiment, one is now in a position to break down the total **g**-tensor components into their individual contributions. It is also appropriate in this section to discuss the nature of the approximations used in the CPKS method.[32]

In the absence of an external electric field, and within the framework of hybrid density functional theory, Neese derived in detail the expressions for the **g**-tensor components. They take the abbreviated form[32]

$$g_{rs} = g_e\delta_{rs} + \Delta g^{RMC}\delta_{rs} + \Delta g_{rs}^{GC} + \Delta g_{rs}^{OZ/SOC} \qquad (1)$$

In brief, $g_e\delta_{rs}$ are the diagonal components of the free electron value of 2.002319, and Δg^{RMC} is the relativistic mass correction to the kinetic energy,

$$\Delta g^{RMC} = \frac{\alpha^2}{S}\sum_{\mu,\nu} P_{\mu,\nu}^{\alpha-\beta}\left\langle \varphi_\mu \left| \frac{1}{2}\nabla^2 \right| \varphi_\nu \right\rangle \qquad (2)$$

Here S is the total spin, $P_{\mu,\nu}^{\alpha-\beta}$ are the spin density matrix elements, and α is the fine structure constant. The angular brackets represent the kinetic energy integrals. Both g_e and Δg^{RMC} are scalar quantities and will only contribute to the diagonal **g**-tensor elements.

According to Stone,[12] Δg_{rs}^{GC} is the diamagnetic correction term,

$$\Delta g_{rs}^{GC} = \frac{1}{2S}\sum_{\mu,\nu} P_{\mu,\nu}^{\alpha-\beta}\left\langle \varphi_\mu \left| \sum_{A,i}\left[\frac{\alpha^2 \quad Z_{eff}^A}{2\,|\bar{r}_i - \bar{R}_A|^3}\right](\bar{r}_A\,\bar{r}_O - \bar{r}_{A,r}\,\bar{r}_{O,s}) \right| \varphi_\nu \right\rangle \qquad (3)$$

This is a second rank tensor and contributes to the total **g** tensor in a fundamentally different way from g_e and Δg^{RMC}. As will be shown later, when the molecule under consideration has high symmetry and no off-diagonal **g** elements, then $\Delta g^{RMC}\delta_{rs}$ and Δg_{rs}^{GC} have different signs and oppose one another. The term in square brackets in eq 3 is the effective spin−orbit coupling constant. Z_{eff}^A is the effective nuclear charge for the *A*th atom and is determined semiempirically.[32] The vector r_i is the position vector of the *i*th electron, similarly, r_A, is its position relative to the *A* nucleus and r_O its position relative to the gauge origin (chosen as the center of charge). From eqs 2 and 3 it is clear that these first-order contributions to the **g**-tensor components are calculated from the spin density.

In eq 1, the cross elements between the orbital-Zeeman and the spin−orbit couplings, $\Delta g_{rs}^{OZ/SOC}$, are the predominant terms[32]

$$\Delta g_{rs}^{OZ/SOC} = \frac{-1}{\beta S}\sum_{\sigma=\alpha,\beta}(-1)^{\delta_{\sigma,\beta}}\sum_i\sum_{a\in\sigma}\frac{\langle \psi^{\sigma(0)}{}_a|\beta \not{l}_r|\psi^{\sigma(0)}{}_i\rangle}{\epsilon_a^{\sigma(0)} - \epsilon_i^{\sigma(0)}} \qquad (4)$$

In eq 4, $\not{l}_{A,s}$ is the Cartesian s component orbital angular momentum on center *A*. An important approximation made in these calculations is that the contributions from the two-electron spin−orbit coupling operators, which effectively screen the electrons, can be eliminated by replacing the nuclear charge, Z^A, on atom *A* by the semiempirical Z_{eff}^A values, parametrized by Koseki et al.[44] Finally, the computations performed here do not take into consideration the gauge dependence of the **g**-tensor components. Provided a basis set of reasonable size is used and the origin is chosen as the center of charge, gauge dependence effects are expected to be small.[32]

Table 2 lists the breakdown of the individual contributions to the computed BzSQ·4CH$_3$OH **g**-tensor components. From this table it is seen that all the tensor components are diagonal.

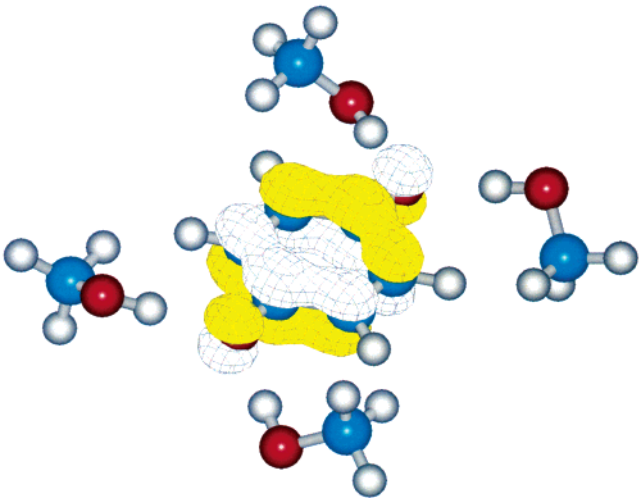

Figure 3. Three-dimensional isosurface of the highest singly occupied b_2 one-electron molecular orbital. The supermolecule in Figure 2 and the SOMO in Figure 3 have the same orientation. The isosurface contour cutoff is 0.05 e/au^3. The BzSQ molecule resides in the *xy* plane and has D_{2h} symmetry while the symmetry of the BzSQ·4CH_3OH supermolecule is D_2.

To rationalize this, one considers first the simpler gas-phase BzSQ, shown in Figure 1. This radical has D_{2h} symmetry and a $^2B_{2g}$ ground state. Contributions to $\Delta g_{xx}^{OZ/SOC}$ arise from the coupling to the excited $^2B_{1g}$ states. Similarly, contributions to $\Delta g_{yy}^{OZ/SOC}$ stem from the coupling to the excited ^2A_g states, and the $\Delta g_{zz}^{OZ/SOC}$ are due to interactions with low lying $^2B_{3g}$ excited states. For a molecule with D_{2h} symmetry, its angular momemtum operators $\hat{\ell}_x$, $\hat{\ell}_y$, and $\hat{\ell}_z$ transform as the B_{3g}, B_{2g}, and B_{1g} irreducible representations, respectively. Since all of these representations are different, then there is no excited state with a particular symmetry that can couple more than one Cartesian component of angular momentum to the $^2B_{2g}$ ground state. This excludes any off-diagonal contributions to $\Delta g_{rs}^{OZ/SOC}$. Similar symmetry arguments also apply to the Δg_{rs}^{GC} terms. Consequently, the total **g** tensor will only have diagonal components.

As shown in Figure 2, when four methanol molecules hydrogen bond to BzSQ the symmetry is reduced from D_{2h} to D_2 and the ground state now has B_2 symmetry. In a radical with D_2 symmetry $\hat{\ell}_x$, $\hat{\ell}_y$,and $\hat{\ell}_z$ transform as the B_3, B_2, and B_1 irreducible representations, respectively. Since these irreducible representations are also all unique, then the total g tensor will have no off-diagonal components in this case too.

Table 2 shows that, at the UB1LYP/AUG-cc-pVTZ level, the contribution of Δg^{RMC} to the g_{xx} component is negative while Δg_{xx}^{GC} is positive and approximately 7.9 times smaller. The $\Delta g_{xx}^{OZ/SOC}$, stems from the coupling with the lowest excited B_{1g} state due to the excitation of the nearest doubly occupied b_{1g} orbital, shown in Figure 4, to the b_{2g} singly occupied molecular orbital (SOMO) in Figure 3. The b_{1g} orbital, in Figure 4, is the out-of-plane π-type orbital that is responsible for the C2C3 and C5C6 double bonds. This form of coupling yields a positive contribution to $\Delta g_{xx}^{OZ/SOC}$ of 0.95267×10^{-4}. It is relatively small and is not enough to compensate for the negative contribution from Δg^{RMC}. As a result, the total g_{xx} component is 2.00218, which is slightly less than the g_e value.

The contributions to the g_{yy} component are more complicated than g_{xx}. While the Δg^{RMC} contribution is the same, Table 2 shows that Δg_{yy}^{GC} is almost double the value of Δg_{xx}^{GC}. The $\Delta g_{yy}^{OZ/SOC}$ contributions are due to the coupling with the low

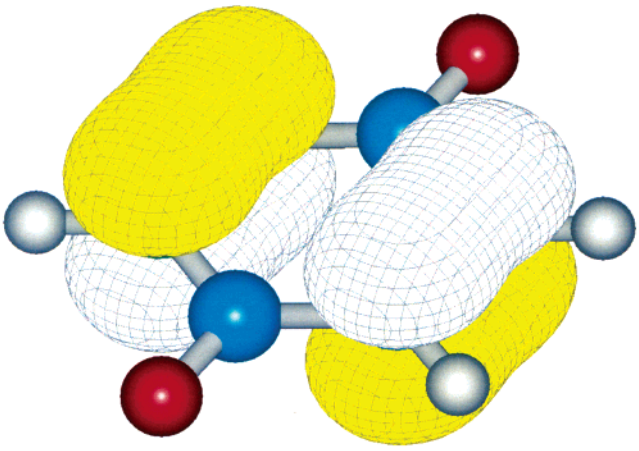

Figure 4. Isosurface of the doubly occupied b_{1g} molecular orbital that couples to the SOMO to form the lowest $^2B_{1g}$ excited state. For the sake of clarity the four methanol molecules are not shown. The isosurface contour cutoff is same as that in Figure 3.

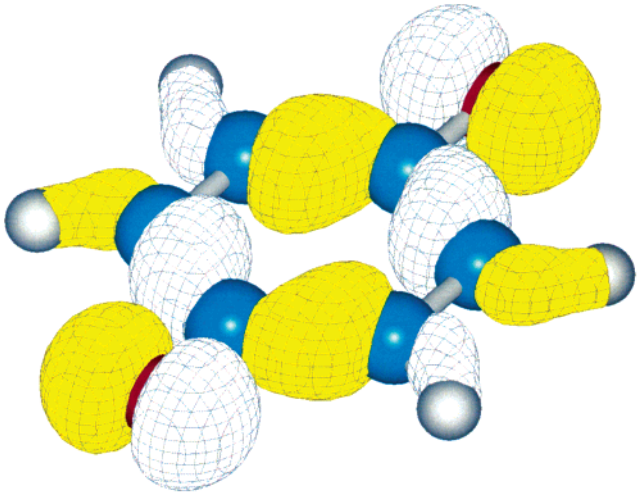

Figure 5. Doubly occupied b_{3g} molecular orbital isosurface. This one-electron molecular orbital couples with the SOMO to form the lowest $^2B_{3g}$ excited state. Its properties are the same as that in Figure 4. The figure clearly illustrates the in-plane $\pi-$type bonding of this orbital.

lying excited states of A_g symmetry. Within a 15 eV energy range there are at least seven A_g excited states that may contribute to the $\Delta g_{yy}^{OZ/SOC}$ term. Four of these states arise from the excitation of doubly occupied σ-type orbitals to the SOMO, while three stem from the excitation of the unpaired electron to a virtual a_g orbital and have the opposite effect. At this stage it is very difficult to perform a thorough analysis and one must rely on the numerical sum of all their contributions. From Table 2 $\Delta g_{yy}^{OZ/SOC}$ is found to be 0.33436×10^{-2}, which is approximately 35 times larger than $\Delta g_{xx}^{OZ/SOC}$. The combined effect of the large $\Delta g_{yy}^{OZ/SOC}$ and Δg_{yy}^{GC} components easily overcomes the negative contribution of Δg^{RMC}, resulting in a total g_{xx} of 2.00548.

Finally, the breakdown of the g_{zz} tensor component is similar to that of the g_{yy}. The Δg_{zz}^{GC} component is more than double the corresponding Δg_{yy}^{GC} component. The $\Delta g_{zz}^{OZ/SOC}$ is mainly due to the coupling with B_{3g} excited states. There are five low lying B_{3g} states, and two of these states arise from the excitation of doubly occupied b_{3g} orbitals. The orbital responsible for the lowest B_{3g} excited state is given in Figure 5 and illustrates its in-plane π-type bonding character. The remaining three excited states are from the excitation of the SOMO to the empty virtual

b_{3g} oribtals. The overall contribution to $\Delta g_{zz}^{OZ/SOC}$ is larger than both $\Delta g_{xx}^{OZ/SOC}$ and $\Delta g_{yy}^{OZ/SOC}$ and boosts the g_{zz} value to 2.00707.

Aside from the g_{zz} values, the EPR−II and AUG-cc-pVTZ basis give g_{xx} and g_{yy} values that are very similar. Thus one may assume that reasonable values can be obtained with a double-ζ basis set at moderate computer times.

All the **g**-tensor computations, listed in Table 1, using the UB1LYP and UPBE0 density functionals yield almost identical results. This seems to indicate that, provided a good HDF is used, its type, whether B1LYP, UPBE0, B3LYP, etc., does not play a significant factor. Neese reached a similar conclusion in his seminal work on smaller organic radicals.[32]

The experimental **g**-tensor components in methanol and 2-propanol are essentially the same. Furthermore, the hydrogen bonding of four 2-propanol molecules to the BzSQ radical anion is expected to be very similar to that occurring in the corresponding BzSQ·4CH_3OH supermolecule. Therefore it is reasonable to expect that the quality of agreement between theory and experiment for the BzSQ·4C_3H_7OH supermolecule should be very similar to that of BzSQ·4CH_3OH.

For the sake of completeness, the hyperfine coupling constants of the BzSQ·4CH_3OH supermolecule ring protons are computed at the UB1LYP/EPR−II level. They are $a^{iso}(^1H) = -2.4480$ G. These are in excellent agreement with those computed by O'Malley using UB3LYP/EPR−II ($a^{iso}(^1H) = -2.2944$ G[25]) and the experimental value of |2.39|Gauss.[4,17,22] This is independent proof that the present calculations result in very accurate electronic structure and spin density distributions.

4. Summary and Conclusions

The **g**-tensor components of the BzSQ radical anion are computed using Neese's CPKS method.[32] When compared to the experimental values, the gas-phase computations overestimate the g_{yy} and g_{zz} while the g_{xx} component is slightly underestimated. The UB1LYP and UPBE0 functionals, which include electron−electron correlation, give better **g**-tensor values than the simpler UHF technique.

The effects of the methanol solvent are first taken into consideration by adopting Tomasi's UAHF−SCRF−PCM method.[34−38] The computations using this method are in better agreement with the experimental ones than the gas-phase results. The second way to take into consideration the solvent is to geometry optimize the BzSQ radical when hydrogen bonded with four methanol molecules to form a BzSQ·4CH_3OH supermolecule. The increase in CO bond lengths and charge redistribution, as a result of the hydrogen bonding, gives very good agreement with experiment. The computed g_{xx}, g_{yy}, and g_{zz} components are now within 110, 220, and 620 ppm of corresponding experimental values, respectively.

The study shows that in all the calculations the EPR−II and Aug-cc-pVTZ basis sets give similar results. Thus one may assume that reasonable values for the **g** tensor can be obtained with a double-ζ basis set at moderate computer times. Furthermore, provided a good HDF is used, its type, whether B1LYP, UPBE0, B3LYP, etc., does not make a significant difference.

In addition to the **g**-tensor components, the isotropic $a^{iso}(^1H)$ of the ring protons are also computed. They are in excellent agreement with their experimental counterparts and those determined previously.[25] This proves that the calculations carried out in this article give a very realistic picture of the electronic structure, magnetic properties, and spin density distribution.

Since the BzSQ radical anion is the simplest basic building block for many quinones, this opens the field for feasibly and accurately computing the magnetic properties and understanding the EPR and ENDOR spectra of hundreds of larger quinones of biological and industrial significance.

Acknowledgment. The Natural Sciences and Engineering Research Council of Canada is gratefully acknowledged for its financial support in the form of individual operating (discovery) grants. This research article is dedicated to Professor J. H. Freed in recognition and appreciation of his long and outstanding career.

References and Notes

(1) Quinones and Quinoidal Radicals in Photosynthesis. Wheeler, R. A. In *Theoretical Biochemistry Processes and Properties of Biological Systems, Theoretical and Computational Chemistry*; Erikson, L. A., Ed.; Elsevier: Amsterdam, 2001; Vol. 9. Trumpower, B. L. In *Function of Quinones in Energy Conserving Systems*; Academic Press: New York, 1982.

(2) Deisenhofer, J.; Norris, J. R. In *The Photosynthetic Reaction Center*; Academic Press: San Diego, 1993; Vols. 1 and 2.

(3) Stone, E. W.; Maki, A. H. *J. Chem. Phys.* **1962**, *36*, 1944.

(4) Freed, J. H.; Gendell, J.; Frankel, G. K. *J. Chem. Phys.* **1962**, *37*, 2832.

(5) Adamo, C.; Barone, V.; Fortunelli, V. *J. Chem. Phys.* **1995**, *102*, 1689.

(6) O'Malley, P. J. *Chem. Phys. Lett.* **1998**, *285*, 99.

(7) Adamo, C.; Barone, V. *Chem. Phys. Lett.* **1997**, *274*, 242.

(8) Mattar, S. M.; Stephens, A. D. *Chem. Phys. Lett.* **1999**, *306*, 249.

(9) Mattar, S. M.; Stephens, A. D. *Chem. Phys. Lett.* **2000**, *319*, 601.

(10) Adamo, C.; di Matteo, A.; Rey, P.; Barone, V. *J. Phys. Chem. A* **1999**, *103*, 3481; di Matteo, A.; Adamo, C.; Cossi, M.; Barone, V.; Rey, P. *Chem. Phys. Lett.* **1999**, *310*, 159.

(11) Improta, R.; Barone, V. *Chem. Rev.* **2003**, in press, and references therein.

(12) Stone, A. J. *Proc. R. Soc. London Ser. A* **1963**, 424. Stone, A. J. *Mol. Phys.* **1963**, *6*, 509. Stone, A. *J. Mol. Phys.* **1964**, *7*, 311.

(13) McWeeny, R. *J. Chem. Phys.* **1965**, *42*, 1717. McWeeny, R. In *Spins in Chemistry*; Academic Press: New York, 1970. McWeeny, R. In *Methods of Molecular Quantum Mechanics*; Academic Press: London, 1992.

(14) Harriman, J. E. In *Theoretical Foundations of Electron Spin Resonance*; Academic Press: New York, 1978.

(15) Pilbrow, J. R. In *Transition Ion Electron Paramagnetic Resonance*; Oxford Science Publications: Oxford, 1990.

(16) Barry, B. A.; Babcock, G. T. *Proc Natl. Acad. Sci. U.S.A.* **1987**, *84*, 7099.

(17) Hales, B. J. *J. Am. Chem. Soc.* **1975**, *97*, 5993.

(18) O'Malley, P. J.; Babcock, G. T. *J. Am. Chem. Soc.* **1984**, *106*, 817.

(19) O'Malley, P. J.; Babcock, G. T. *J. Am. Chem. Soc.* **1986**, *108*, 3995.

(20) O'Malley, P. J.; Babcock, G. T. *J. Chem. Phys.* **1984**, *80*, 3912.

(21) Borbat, P. B.; Crepeau, R. H.; Freed, J. H. *J. Magn. Res.* **1997**, *127*, 155.

(22) Burghauss, O.; Plato, M.; Roher, M.; Mobius, K.; MacMillan, F.; Lubitz, W. *J. Phys. Chem.* **1993**, *97*, 7639.

(23) Grinberg, O. Ya; Dubinski, A.; Shuvalov, V. F.; Oranskii, L. A.; Kurochkin, V. I.; Lebedev, Ya. S. *Dokl. Phys. Chem.* **1976**, *230*, 923.

(24) Lynch, W. B.; Earle, K.; Freed, J. H. *Rev. Sci. Instrum.* **1988**, *59*, 1345. Budil, D. E.; Earle, K. A.; Lynch, W. B.; Freed, J. H. In *Advanced EPR Applications in Biology and Biochemistry*; Hoff, A., Ed.; Elsevier: Amsterdam, 1989; Ch. 8, p 307.

(25) O'Malley, P. J. *Chem. Phys. Lett.* **1996**, *262*, 797.

(26) Neese, F. *Int. J. Quantum Chem.* **2001**, *83*, 104.

(27) Lushington, G. H.; Bundgen, P.; Grein, F. *Int. J. Quantum Chem.* **1995**, *55*, 377. Bruna, P. J.; Grein, F. *Int. J. Quantum Chem.* **2000**, *77*, 324.

(28) Vahtras, O.; Minaev, B.; Agren, H. *Chem. Phys. Lett.* **1997**, *281*, 186.

(29) Schrekenbach, G.; Zeigler, T. *Theor. Chem. Acc.* **1998**, *99*, 71.

(30) Schrekenbach, G.; Zeigler, T. *J. Phys. Chem.* **1997**, *101*, 3388. van Lenthe, E.; Wormer, P.; van der Avoird, A. *J. Chem. Phys.* **1997**, *107*, 2488.

(31) Patchkovskii, S.; Zeigler, T. *J. Chem. Phys.* **1999**, *111*, 5730. Patchkovskii, S.; Zeigler, T. *J. Phys. Chem A* **2001**, *105*, 5490.

(32) Neese, F. *J. Chem. Phys.* **2001**, *115*, 11080.

(33) Engstrom, M.; Vahtras, O.; Agren, H. *Chem. Phys.* **1999**, *243*, 263.

(34) Foresman, J. B.; Frisch, A. In *Exploring Chemistry with Electronic Structure Models*; Gaussian Inc.: Pittsburgh, PA, 1996 and references therein.

(35) De Luca, G.; Mineva, T.; Russo, N.; Sicilia, E.; Toscano, M. In *Advances in Density Functional Methods*; Chong, D. P., Ed.; World Scientific Publishing: Singapore, 1995.

(36) Miertus, S.; Tomasi, J. *J. Chem. Phys.* **1982**, *65*, 239. Tomasi, J.; Persico, M. *Chem. Rev.* **1994**, *94*, 2027.

(37) Cossi, M.; Barone, V.; Cammi, R.; Tomasi, J. *Chem. Phys. Lett.* **1996**, *255*, 327.

(38) Barone, V.; Cossi, M.; Tomasi, J. *J. Chem. Phys.* **1997**, *107*, 3210. Cossi, M.; Scalmani, G.; Rega, N.; Barone, V. *J. Chem. Phys.* **2002**, *117*, 43.

(39) Gaussian 03, Revision A.1, Frisch, M. J., Trucks, G. W., Schlegel, H. B., Scuseria, G. E., Robb, M. A., Cheeseman, J. R., Montgomery, J. A., Jr., Vreven, T., Kudin, K. N., Burant, J. C., Millam, J. M., Iyengar, S. S., Tomasi, J., Barone, V., Mennucci, B., Cossi, M., Scalmani, G., Rega, N., Petersson, G. A., Nakatsuji, H., Hada, M., Ehara, M., Toyota, K., Fukuda, R., Hasegawa, J., Ishida, M., Nakajima, T., Honda, Y., Kitao, O., Nakai, H., Klene, M., Li, X., Knox, J. E., Hratchian, H. P., Cross, J. B., Adamo, C., Jaramillo, J., Gomperts, R., Stratmann, R. E., Yazyev, O., Austin, A. J., Cammi, R., Pomelli, C., Ochterski, J. W., Ayala, P. Y., Morokuma, K., Voth, G. A., Salvador, P., Dannenberg, J. J., Zakrzewski, V. G., Dapprich, S., Daniels, A. D., Strain, M. C., Farkas, O., Malick, D. K., Rabuck, A. D., Raghavachari, K., Foresman, J. B., Ortiz, J. V., Cui, Q., Baboul, A. G., Clifford, S., Cioslowski, J., Stefanov, B. B., Liu, G., Liashenko, A., Piskorz, P., Komaromi, I., Martin, R. L., Fox, D. J., Keith, T., Al-Laham, M. A., Peng, C. Y., Nanayakkara, A., Challacombe, M., Gill, P. M. W., Johnson, B., Chen, W., Wong, M. W., Gonzalez, C. and Pople, J. A. Gaussian, Inc.: Pittsburgh, PA, 2003.

(40) Perdew, J. P.; Burke, K.; Ernzerhof, M. *Phys. Rev. Lett.* **1997**, *78*, 1396.

(41) Adamo, C.; Barone, V. *J. Chem. Phys.* **1999**, *110*, 6158.

(42) Barone, V. In *Recent Advances in Density Functional Methods, Part I*; Chong, D. P., Ed.; World Scientific: Singapore, 1996.

(43) Wilson, A.; van Mourik, T.; Dunning, T. H., Jr. *J. Mol. Struct. (THEOCHEM)* **1997**, *388*, 339.

(44) Koseki, S.; Schmidt, M. W.; Gordon, M. S. *J. Phys. Chem.* **1992**, *96*, 10768.